Frequency-modulated excitation of a two-level atom

Michael W. Noel, W. M. Griffith, and T. F. Gallagher
Department of Physics, University of Virginia, Charlottesville, Virginia 22901
(Received 19 September 1997)

We present a detailed experimental study of the frequency-modulated excitation of a two-level atom, using a microwave field to drive transitions between two Rydberg Stark states of potassium. In the absence of a modulation the interaction is the standard model of the Rabi problem, producing sinusoidal oscillations of the population between the two states. In the presence of a frequency modulation of the interacting field, however, the time evolution of the system is significantly modified, producing square wave oscillations of the population, sinusoidal oscillations at a different frequency, or even sinusoidal oscillations built up in a series of stair steps. The three responses described above are each found in a different regime for the frequency of the modulation with respect to the unmodulated Rabi frequency: the low-, high-, and intermediate-frequency regimes, respectively. [S1050-2947(98)03209-0]

PACS number(s): 42.50.Hz, 32.80.−t, 32.30.Bv, 42.50.Md

I. INTRODUCTION

The two-level atom is perhaps the most basic system in which to study the interaction between a quantum system and an electromagnetic field. In the simplest case of the interaction with a continuous monochromatic field, familiar Rabi oscillations of the population between the two states are seen in the temporal evolution of the system [1–4]. In the frequency domain the same simple interaction is manifested in the well-known three-peaked fluorescence spectrum [5–7]. This spectrum is a result of the dressing of the atomic states by the strong resonant field [8], which appears as the Autler-Townes doublet when probed with a second weak laser [9–12].

When the amplitude of the exciting field is modulated the atomic response becomes more complicated. For instance, the excitation with a 100% amplitude-modulated field leads to resonances in the steady-state inversion when the modulation frequency is at a subharmonic of the Rabi frequency [13]. There is also a more complicated beating in the system's time evolution, which has a strong dependence on the initial phase of the modulation [14–16]. Finally, the resonance fluorescence [17–21] and Autler-Townes [22,23] spectra from an amplitude modulated interaction are more complicated than the monochromatic case, containing a series of peaks separated by the modulation frequency whose widths alternate.

In the case of a frequency-modulated excitation, many interesting effects have been predicted and observed. To date, most of the experimental work with such an interaction has focused on the development of the very sensitive technique of frequency-modulation spectroscopy [24,25]. Recent theoretical exploration of the time evolution of a two-level system driven by a frequency-modulated field has revealed square-wave oscillations of the population [26,27] as well as more complicated and phase-dependent structures [28,29]. The resonance fluorescence [30] and Autler-Townes [31] spectra for a frequency-modulated interaction have also been considered, revealing additional sidebands in the spectrum, chaotic behavior of the spectrum for two frequency modulation, and simultaneously forbidden resonances.

In this paper we present a detailed experimental study of the frequency-modulated excitation of a two-level atom. We focus on the transient dynamics of the system for a wide range of parameters of the modulation. For our system we used two well isolated states of a potassium Rydberg atom in an electric field. They are adiabatically connected to the $21s$ and $19f$ zero-field states, and we shall label the states $21s$ and $19f$ as shown in Fig. 1. The $21s$ state shifts quadratically in energy as a function of the static electric field and the $19f$ state has a linear Stark shift. The static electric field was used to tune the level separation into resonance with a microwave photon that coupled the two states. Rather than modulate the frequency of this microwave photon directly we instead chose to apply a second low-frequency field. This radio-frequency (rf) field in combination with the static electric field had the effect of modulating the energy separation between the two states. Modulation of the level separation is formally equivalent to modulation of the exciting field frequency, and is much more convenient in this system of Stark states.

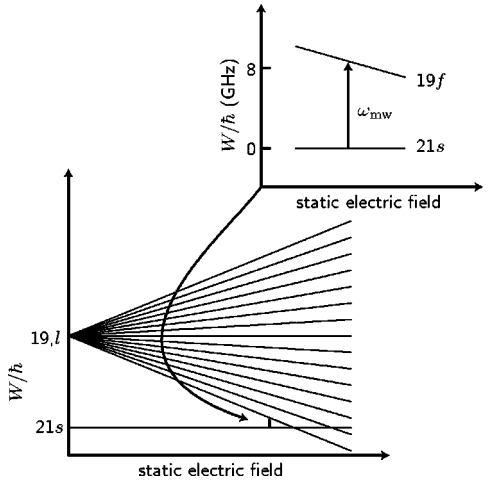

FIG. 1. Stark states of a potassium Rydberg atom. The static electric field was used to tune the $19f-21s$ level separation into resonance with the 8-GHz microwave photons. The inset shows the two well isolated states that make up our two-level atom.

 © 1998 The American Physical Society

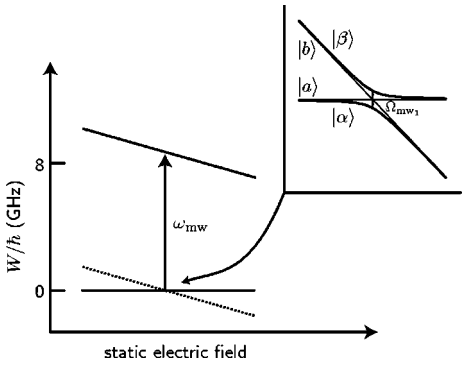

FIG. 2. Dressed states of an atom in combined static and microwave fields. The inset shows the avoided crossing that occurs due to the coupling between the two states.

It is natural to compare the frequency of the modulating field to the Rabi frequency of the resonant transition driven by the microwave field in the absence of the modulation, and we have studied the effect of this modulating field over a wide range of frequencies. We begin with the case in which the modulation frequency is slow compared to the Rabi frequency. Next, we move to the limit of fast modulation. We then consider the case of intermediate modulation frequencies and draw some connections between the two limiting cases. A second parameter that is also very important in determining the system's evolution is the amplitude of the modulation. Within each of the sections outlined above we discuss the range of modulation amplitudes used along with their influence on the observed dynamics.

II. SLOW MODULATION

A. Microwave dressed state

We begin by considering the limit in which the modulation frequency is small compared to the resonant Rabi frequency driven by the microwave field in the absence of modulation. For this case we look at the dressed states of the atom plus microwave field and then consider the effect of the modulating field on these dressed states.

The theory of dressed or Floquet stark states of an atom in combined static and microwave fields has been presented in several papers [4,32] with the main result that, at a given microwave multiphoton resonance (we use the single photon resonance), the problem is reduced to two states coupled by the interaction, Ω_{mw_q}, where q refers to the number of photons absorbed. The inset of Fig. 2 shows the states of our system after having subtracted the energy of one microwave photon from the upper state. In the absence of the microwave interaction, these two states cross, and we refer to them as uncoupled states $|a\rangle$ and $|b\rangle$. In the presence of the microwave interaction, the Schrödinger equation at the one-photon resonance is

$$i\begin{bmatrix}\dot{a}\\ \dot{b}\end{bmatrix}=\begin{bmatrix}W_a & \frac{\Omega_{\mathrm{mw}_1}}{2}\\ \frac{\Omega_{\mathrm{mw}_1}}{2} & W_b\end{bmatrix}\begin{bmatrix}a\\ b\end{bmatrix}, \tag{1}$$

where a and b are the amplitudes and $W_a=0$ and $W_b=-k(E_{\mathrm{static}}-E_1)$ are the energies of the states $|a\rangle$ and $|b\rangle$. Here we have neglected the quadratic Stark shift of the $21s$ state, which has little effect for the field strengths used in this experiment, so $k=549$ MHz/(V/cm) is the relative slope of the $21s$ and $19f$ states at the one-photon resonance. E_{static} is the static electric field and $E_1=289$ V/cm is the field at which one microwave photon is in resonance with the level separation.

The energies, $W_\alpha=(W_b-\sqrt{W_b^2+\Omega_{\mathrm{mw}_1}^2})/2$ and $W_\beta=(W_b+\sqrt{W_b^2+\Omega_{\mathrm{mw}_1}^2})/2$ of the dressed states, $|\alpha\rangle$ and $|\beta\rangle$ are found by simply diagonalizing the time-independent Hamiltonian in Eq. (1). The dressed states form an avoided crossing whose separation at the one-photon resonance is Ω_{mw_1}. A general expression for the separation of the dressed state avoided crossing at the q photon resonance is given in Ref. [32] as

$$\Omega_{\mathrm{mw}_q}=\Omega_{\mathrm{static}}J_q\left(\frac{kE_{\mathrm{mw}}}{\omega_{\mathrm{mw}}}\right) \tag{2}$$

where Ω_{static} is the size of the static field avoided crossing, J_q is a Bessel function of order q, E_{mw} is the microwave field amplitude, and ω_{mw} is the microwave frequency.

Next we consider the effect of adding the rf modulating field to the upper state energy along with the static electric field, $W_b=-k[E_{\mathrm{static}}-E_{\mathrm{rf}}\cos(\omega_{\mathrm{rf}}t)-E_1]$. We set the static field to the one-photon microwave resonance $E_{\mathrm{static}}=E_1$ and use a sinusoidal modulation that begins as a cosine and whose amplitude is large, so that the system will initially be off resonance and far from the avoided crossing. For these conditions the lower dressed state $|\alpha\rangle$ is initially made up of mostly the lower uncoupled state, $|a\rangle$, which is the state that we initially populate, so $\alpha(t=0)\approx 1$. Since the modulation is slowly changing, the population will remain in the lower dressed state as the microwave field is swept through resonance. On the other side of the crossing the lower dressed state is composed mostly of uncoupled state $|b\rangle$, so the two-level system makes a transition between the two uncoupled states in the familiar method of adiabatic rapid passage [33,34]. Each time the sinusoidal modulation sweeps the system through resonance the population will jump between uncoupled states, so the population of state $|b\rangle$ as a function of time oscillates like a square wave with a period equal to that of the modulating field.

B. Square-wave population oscillations

We measured the time evolution of the two-state system in the presence of a slow modulation as follows. The atom was prepared in the $21s$ state with a pair of laser pulses. The modulation and microwave fields were then turned on to interact with the atom. By adjusting the phase of the rf modulating field relative to the start of the microwave pulse we started with the system initially off resonance. The length of the microwave pulse was then scanned from 0 to 256 ns in 1 ns steps and the upper state population measured after each step.

The heart of the experimental apparatus is shown in Fig. 3. The interaction between the atoms and the microwave and rf fields took place inside a piece of WR137 waveguide. The

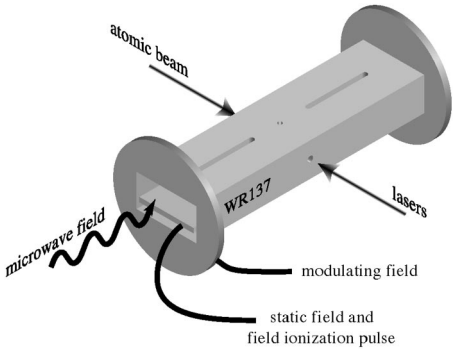

FIG. 3. The portion of the experimental apparatus in which the interaction takes place. It is a piece of WR137 waveguide with a septum and holes to couple in the fields, lasers, and atoms used in the experiment.

potassium atoms effusing from a resistively heated oven entered the waveguide through a small hole in one of its sides. The two nanosecond dye laser beams, tuned to excite the atom from the $4s$ to $4p$ and $4p$ to $21s$ states entered the waveguide through a hole on the opposite side.

The 8-GHz microwave field was coupled into and out of the waveguide using waveguide to coaxial adapters. By pulsing the microwave field with a square envelope, the interaction time with the microwave field was varied. To generate this variable length microwave pulse we double mixed (using Watkins-Johnson M14A mixers) the continuous wave output of a Hewlett Packard HP8350B microwave sweeper with a digitally programmable pulse from a Tektronix AWG2040 arbitrary wave-form generator. The resulting microwave pulse was amplified and sent into the waveguide. The output of the waveguide was attenuated and terminated with a microwave detector.

The AWG2040 also triggered a Wavetek model 22 function generator, which produced a sinusoidal field at 10.25 MHz whose phase was locked to the beginning of the microwave pulse. By isolating the center section of the waveguide from ground with thin teflon spacers at each end, we were able to apply the modulating field directly to the outside of the waveguide.

Inside the waveguide was a copper septum to which we applied the static electric field, used to tune to the microwave resonance, and a field-ionization pulse used to detect the upper $(19f)$ state population. The field-ionization pulse was applied after the microwave interaction, and its amplitude was adjusted so that it only ionized atoms that were in the $19f$ state, not those in the $21s$ state. The $19f$ ions then passed through a small hole in the top of the waveguide and impinged upon a microchannel plate detector.

The time evolution of the two-level atom driven by the microwave field both with and without the slow modulating field is shown in Fig. 4. In Fig. 4(a), with the modulation turned off, we see the standard sinusoidal Rabi oscillations at a frequency of 81 MHz for this microwave field strength. In Fig. 4(b), with the modulation on at a frequency of 10.25 MHz ($\omega_{\rm rf} \approx \frac{1}{8}\Omega_{\rm mw_1}$) and amplitude of approximately 0.6 V/cm ($kE_{\rm rf} = 329$ MHz), we see square rather than sinusoidal oscillations of the excited-state population, the sharp jumps occurring each time the modulating field sweeps the system through resonance with the microwave field.

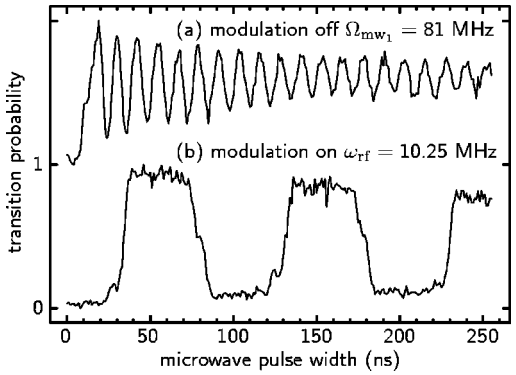

FIG. 4. Time evolution of the two-level atom (a) without the rf modulation and (b) with the rf modulation.

Although we used a 50-Ω resistor to terminate the waveguide section to ground, there was also a large capacitance at the ends of the waveguide, resulting in an impedance mismatch for the rf signal and a corresponding uncertainty in our estimate of the rf amplitude experienced by the atoms. In the low-frequency regime, however, the atomic response should be insensitive to the modulation amplitude. To verify this we took several scans at rf amplitudes ranging from 0.4 to 0.8 V/cm ($kE_{\rm rf} = 220$ to 440 MHz) and saw nearly identical responses.

III. FAST MODULATION

A. rf multiphoton resonances

For a fast modulating field we take a different theoretical approach. In this case we consider the states of the atom dressed by both the microwave and rf fields. In the previous section it was stated that the atom plus microwave field interaction produces dressed states with an avoided crossing that is identical to a static field avoided crossing. Dressing these states again with the rf field is straightforward. In fact, this analysis is identical to the Floquet description given by Stoneman *et al.* [32]. The result of this analysis is that the upper state is broken up into a carrier and series of sidebands

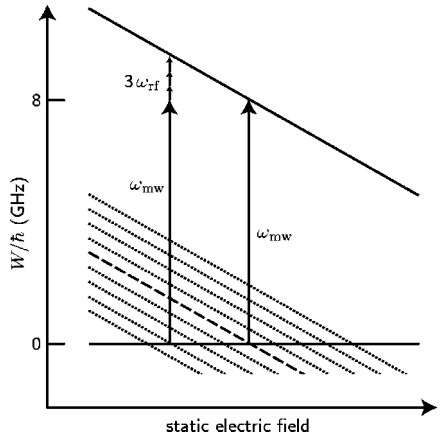

FIG. 5. Dressed states of the atom plus microwave field plus rf field system. The rf field produces a series of sideband resonances to which we can tune using the static electric field. At each of these sidebands there is an avoided crossing whose size is a function of the amplitude of the modulating field.

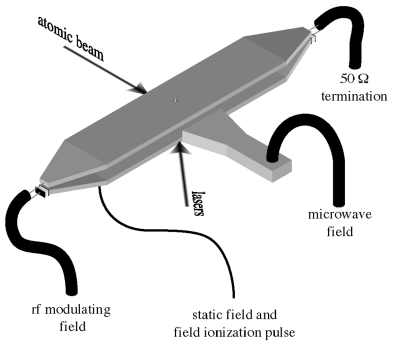

FIG. 6. Portion of the experimental apparatus in which the interaction takes place. The rf field is sent along the transmission line and the microwave field radiates out of the horn.

as shown in Fig. 5, just as a frequency-modulated radio signal consists of a carrier and sidebands.

In the limit where the modulation frequency is large compared to Ω_{mw_1} these rf resonances are well separated and each forms its own avoided crossing. The separation between dressed states, or equivalently, the rf multiphoton Rabi frequency at these avoided crossings is given by

$$\Omega_{\mathrm{rf}_q} = \Omega_{\mathrm{mw}_1} J_q\left(\frac{kE_{\mathrm{rf}}}{\omega_{\mathrm{rf}}}\right), \tag{3}$$

where J_q is again a Bessel function of order q, but now q refers to the number of rf photons being absorbed. E_{rf} and ω_{rf} are the rf field amplitude and frequency, respectively. By adjusting the static electric field we can tune to each of these rf avoided crossings and study them individually.

B. Experiment

In the limit of fast modulation we again expect sinusoidal oscillations of the population, but now at an effective Rabi frequency given by Eq. (3) as a function of modulation amplitude. We were able to map out these Bessel functions by measuring the rf Rabi frequency Ω_{rf_q} at a given rf resonance q for different rf field amplitudes E_{rf}. The Rabi frequencies were again measured by scanning the microwave pulse width for each fixed modulation amplitude and recording the time evolution of the upper state.

Application of the much higher modulation frequencies necessary in this limit required a very different experimental arrangement, which is shown in Fig. 6. In this case the interaction took place in the center of an rf transmission line. This transmission line was designed to maintain 50-Ω impedance over a broad range of frequencies (from less than 50 MHz to over 2 GHz) by keeping the proper height to width ratio over the length of the line. The rf signal was coupled into and out of the transmission line at each end using 50-Ω coaxial cables. The center conductor of each cable was connected to the top plate of the line and the outer conductor was coupled to the lower plate through an rf capacitor. The purpose of the blocking capacitors was to isolate the rf electronics from the high voltage static electric field and slowly varying field-ionization pulse, which were applied directly to the bottom plate of the transmission line.

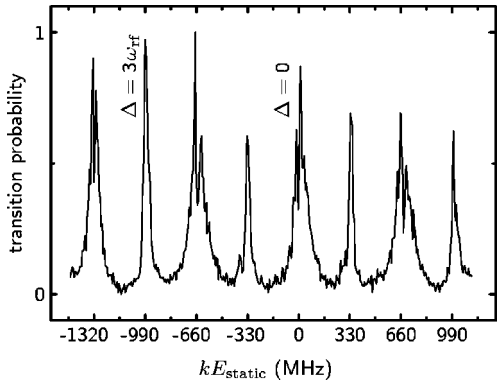

FIG. 7. Scan of the static electric field (plotted in frequency units) for fixed microwave and rf amplitude and pulse width. The carrier resonance is labeled $\Delta = 0$ and the third sideband is labeled $\Delta = 3\omega_{\mathrm{rf}}$. For the narrow resonances we are near a zero of the Bessel function that is determining the transition strength for that resonance. The opposite is true for the broad resonances. Since the microwave pulse width was only 128 ns the system had not yet reached its steady-state value for the inversion so there is some structure in the broad resonances.

In this case a 9-GHz microwave field was introduced into the interaction region between the plates of the transmission line using a microwave horn. The horn was designed to provide good impedance matching to free space by flaring it in the horizontal direction. In order to efficiently couple most of the microwave power into the region between the plates of the rf transmission line, the vertical dimension of the horn was designed to match the vertical separation of the plates.

The atomic beam entered the transmission line opposite the horn and the lasers entered at an angle to cross the atomic beam underneath a 0.5-mm hole in the upper plate. Ions were extracted through this small hole and collected on a microchannel plate detector.

To create the variable length microwave pulse for this arrangement we used a Stanford Research Systems DG535 programmable pulse generator to mix with the cw microwaves. Here the AWG2040 was triggered with the DG535 and programmed to generate the rf modulation frequency.

We began by fixing the amplitude of the microwave and rf fields and scanning the static electric field to look at the rf multiphoton resonances. The absorption spectrum in Fig. 7 shows the carrier and several sideband resonances. In this case the microwave amplitude was set to yield a microwave Rabi frequency of $\Omega_{\mathrm{mw}_1} = 156$ MHz. The rf frequency was set to $\omega_{\mathrm{rf}} = 330\ \mathrm{MHz} \approx 2\Omega_{\mathrm{mw}_1}$ and its amplitude to $E_{\mathrm{rf}} = 4.13$ V/cm ($kE_{\mathrm{rf}} = 2.27$ GHz). For these parameters the rf resonances were well separated so the high-frequency approximation of this section is valid.

The variation in the widths of the peaks in Fig. 7 is due to the variation in the rf Rabi frequencies defined by Eq. (3). For this particular rf field amplitude Ω_{rf_1} and Ω_{rf_3} are small, leading to narrow resonances where as Ω_{rf_0} and Ω_{rf_2} are large leading to broad peaks. Also, since the microwave pulse width for this scan was only 128 ns the system had not yet reached its steady-state value for the inversion so there is some structure in the broad resonances.

Next we fixed the static field at an rf resonance and measured Rabi oscillations for various rf field amplitudes. In Fig.

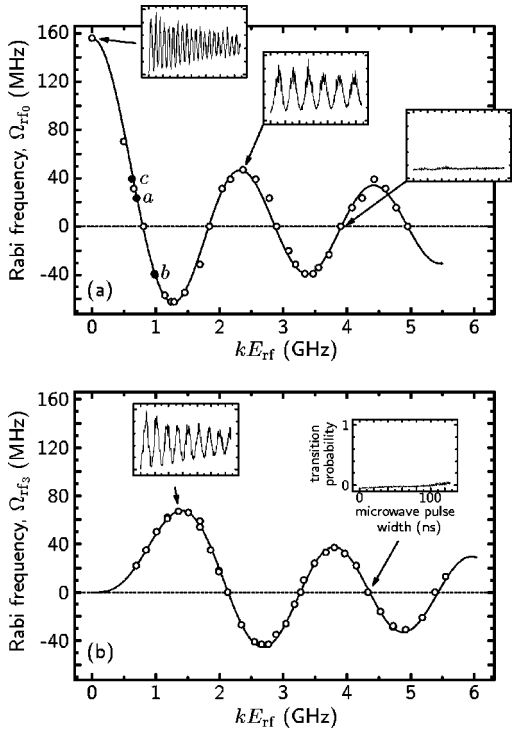

FIG. 8. A compilation of data for various rf amplitudes with the static field tuned to (a) the carrier and (b) the third sideband resonance. The insets show the Rabi oscillation at a few specific modulation amplitudes from which we measured the Rabi frequencies. The axes on all of the insets are scaled identically to the one that is labeled. The points explicitly labeled *a*, *b*, and *c* are modulation amplitudes that also appear in Figs. 9 and 10.

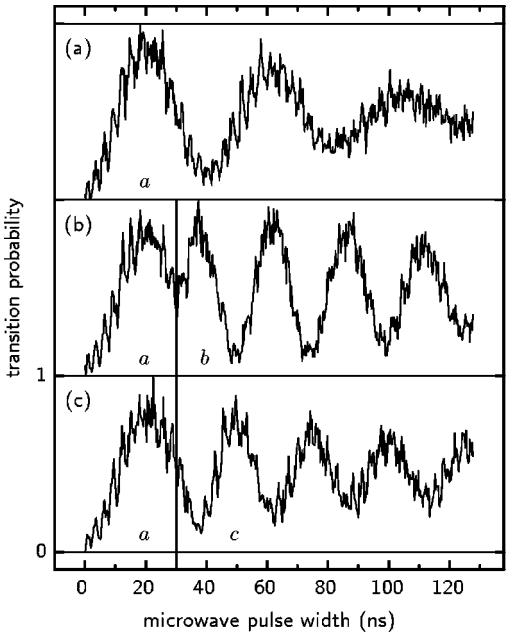

FIG. 9. Curve (a) shows the Rabi oscillations for a modulation amplitude at the highlighted point labeled *a* in the previous figure. In (b) and (c) there is a vertical line showing the time at which the rf amplitude was suddenly switched during the time scan to the value labeled *b* and *c*, respectively, in the previous figure.

8 we show the compilation of such measurements along with the theoretically predicted Bessel functions for two rf resonances, the carrier and the third sideband. The insets show sinusoidal Rabi oscillations at a few specific rf amplitudes. These data show excellent agreement with the theoretical prediction given in Eq. (3). The only parameter used to fit these data was the Rabi frequency at $E_{rf}=0$, which we measured to be 156 MHz, since we did not have an accurate measure of the microwave power at the interaction region. The rf amplitude was determined by measuring the voltage of the rf wave form on an oscilloscope, taking into account losses in the cables and transmission line, and converting this to a field using the known spacing between the plates of the rf transmission line. Using this calibration resulted in excellent agreement between the location of the measured zeros of the Rabi frequency and the theoretical prediction for the zeros of the Bessel function.

The small size of the interaction region (defined by the intersection of the lasers, atomic beam, and projection of the extraction hole) leads to excellent static and microwave field homogeneity. The decay of the rf Rabi oscillations seen in the insets in Fig. 8 is due to the residual microwave field inhomogeneity. With this setup we were able to measure frequencies as low as 10 MHz. We also show data taken at the rf amplitudes for which Ω_{rf_0} and Ω_{rf_3} are zero. At these amplitudes the population remained in its initial state during the entire scan of the microwave pulse width.

Bessel functions oscillate in sign, implying that for some rf amplitudes the rf Rabi frequency is negative. We have plotted some of our observed Rabi frequencies as being negative, although we cannot, using the method described, determine the sign of the Rabi frequency. However, we were able to verify that the Rabi frequency does change sign for modulation amplitudes on opposite sides of a zero of the Bessel function using a different method.

To measure this sign change we focus on the three modulation amplitudes noted as *a*, *b*, and *c* in Fig. 8(a). Figure 9(a) shows the time evolution for the rf amplitude at the point labeled *a* in Fig. 8. In Figs. 9(b) and 9(c) we changed the amplitude of the rf modulating field at a fixed time during a scan of the microwave pulse width. Using the AWG2040, this sinusoidal wave form at 330 MHz with a sudden change in amplitude was easily generated. We chose this time to be 3/4 of the Rabi period for the initial rf amplitude. When we changed the modulation amplitude we not only saw the Rabi period change, but also a 180° phase shift, which depended on whether or not the sign changed. More specifically, if the Rabi frequency had changed sign as in Fig. 9(b), the population of the upper state increased rather than continuing to decrease, whereas for no sign change as in Fig. 9(c) the population continued to decrease.

In Fig. 9 we also see that after the change in rf amplitude, the amplitude of the Rabi oscillations in curve (b) are larger than in curve (c). To explore this effect further we moved the position of the rf amplitude change much later in time. In fact, we waited until the different atoms in our ensemble had completely dephased and washed out the Rabi oscillations. Now when the sign of the Rabi frequency was changed we reversed the effect of this dephasing and saw an echo in the Rabi oscillations (see Fig. 10). This is in many ways analogous to a photon echo [35] or nutation echo [36] seen in optical resonance experiments, as well as the familiar spin echoes [37] and rotary echoes [38] seen in nuclear magnetic resonance.

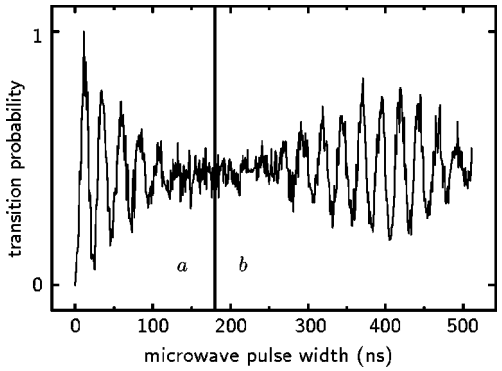

FIG. 10. Here the amplitude of the rf field was suddenly switched from *a* to *b*, but at a much later time than in the previous figure. This allowed the ensemble to completely dephase before the sign change and then rephase in the form of an echo after the sign change of the Rabi frequency.

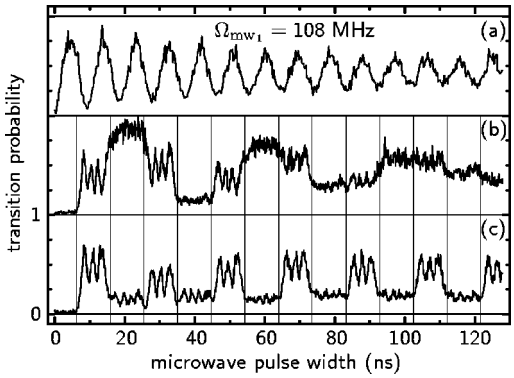

FIG. 11. In curve (a) we show a Rabi oscillation of 108 MHz in the absence of frequency modulation. For (b) and (c) the modulation was turned on with a frequency of 52 MHz and an amplitude of 0.92 V/cm and 0.78 V/cm, respectively. The vertical lines are the times at which the rf field sweeps the system through resonance with the microwave field. In (b) we see constructive interference at the second avoided crossing and in (c) we see destructive interference.

By considering the Bloch vector rotating on a sphere it is easy to see where the echo comes from [39]. For an on-resonant interaction the Bloch vector rotates through both poles of the sphere at the resonant Rabi frequency. For an atom that is slightly detuned from resonance (mostly due to field inhomogeneities in our case) the Bloch vector does not quite reach the north pole (complete inversion) and it rotates at a slightly faster frequency, the generalized Rabi frequency. Since we excite many different atoms, each with slightly different detunings and thus different generalized Rabi frequencies, we see the amplitude of the Rabi oscillations for the ensemble decay as the different frequencies dephase. By changing the sign of the Rabi frequency we change the direction of rotation of each of the Bloch vectors in the ensemble. This effectively reverses time, winding each Bloch vector back up to its initial starting point, where the amplitude of the Rabi oscillations for the ensemble is again a maximum.

IV. INTERMEDIATE MODULATION

A. Stair step population oscillations

With this understanding of the two limits of modulation frequency we turn to the intermediate frequency regime, where the frequency is too slow for the rf resonances to be well isolated and yet too fast for the population to adiabatically follow the microwave dressed states.

Here we used an experimental arrangement that was identical to that described in Sec. III B and again focused on the time evolution of the system. Figure 11(a) shows microwave Rabi oscillations at a frequency of $\Omega_{mw}=108$ MHz with the modulating field off. In Figs. 11(b) and 11(c) we show the time evolution for two specific modulation amplitudes and a modulation frequency of $\omega_{rf}=52$ MHz$\approx\frac{1}{2}\Omega_{mw_1}$. For Fig. 11(b), we see an oscillation at $\approx$25 MHz built up in a series of steps that occur at twice the modulation frequency. It is similar to a Rabi oscillation in that the transition probability oscillates over time. The curve in Fig. 11(c) is more like the square population oscillations seen in Fig. 4 except that the population is never completely transferred to the upper state.

A qualitative understanding of this behavior is gained using a Landau-Zener phase accumulation model. In this model we consider the microwave dressed states introduced in Sec. II A. In Fig. 12 we show the dressed states as a function of time in the sinusoidal modulating field. As the rf field sweeps the system through resonance at the dressed state avoided crossing, there is a nonzero transition amplitude for making a diabatic transition to the other state. The system is now in a superposition of the two dressed states, so when the avoided crossing is traversed a second time there will be interference between the two transition amplitudes. The result of this interference depends on the relative phase accumulated by the two states during their evolution in between crossings. In Fig. 11(b) the rf amplitude was chosen to result in constructive interference (a single cycle transition probability of one), whereas in Fig. 11(c), the interference was destructive (a single cycle transition probability of zero). Different rf amplitudes and frequencies would result in different half and single cycle transition probabilities, with consequently more complicated time dependence. The choice of parameters that produced Figs. 11(b) and 11(c) makes the time dependence particularly simple since after one cycle, the population is entirely in one state or the other. As an example of a different choice of conditions, an rf frequency of $\Omega_{mw_1}/2$ and a large rf amplitude would result in small half cycle transition probabilities and discretized Rabi oscillations, with stair

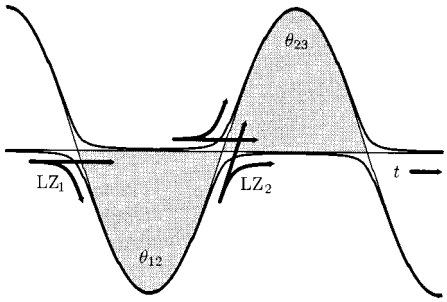

FIG. 12. Schematic representation of the Landau-Zener phase accumulation model. At the first avoided crossing the population splits between states. At subsequent avoided crossings the population following the two paths can interfere.

steps occurring at every half rf cycle. Unfortunately, these parameters were unattainable with our apparatus.

This behavior is much like a multilayer dielectric stack in optics, where each dielectric interface corresponds to an avoided crossing in our system. The light propagating through such a dielectric stack is split at each interface depending on the reflection coefficient. The result of the interference at each interface depends not only on this reflection coefficient, but also on the phase accumulated by the interfering beams in between interfaces.

B. Landau-Zener model

The model outlined in the previous section is developed in more detail here. The model is used in this section to explain the atomic response in this intermediate frequency regime, and in the next section it is used to make some connections between the high- and low-frequency regimes.

The first Landau-Zener transition shown in Fig. 12 is described by the unitary matrix [40–42],

$$U_{\mathrm{LZ}_1}=\begin{pmatrix} \sqrt{P} & -\sqrt{1-P}e^{-i\phi} \\ \sqrt{1-P}e^{i\phi} & \sqrt{P} \end{pmatrix}. \tag{4}$$

Here ϕ is the phase accumulated during this transition and P is the Landau-Zener probability for making a diabatic transition [43],

$$\phi=\frac{\pi}{4}-\delta\ \ln\ \delta+\delta+\arg\ \Gamma(1-i\delta), \tag{5}$$

$$P=\exp(-2\pi\delta), \tag{6}$$

$$\delta=\frac{\Omega_{\mathrm{mw}_1}^2}{4\ dW/dE dE/dt}. \tag{7}$$

The rate of change of the states' energy with respect to the electric field is $dW/dE=k$ and the rate of change of the field with respect to time is $dE/dt=\omega_{\mathrm{rf}}E_{\mathrm{rf}}$ when at the crossing. Using the experimental parameters for Figs. 11(b) and 11(c) we find that $P\approx 0.5$, leaving the system in a superposition of the two states after a half cycle of rf. This transition probability is in good agreement with the size of the first step seen in Figs. 11(b) and 11(c).

Next, we model the evolution between the first and second crossings as a simple phase accumulation by the two states, using the propagation matrix,

$$U_{\theta_{12}}=\begin{pmatrix} 1 & 0 \\ 0 & e^{-i\theta} \end{pmatrix}. \tag{8}$$

Note that we have chosen the special case in which the microwave field is on resonance so the sinusoidal oscillation of state $|b\rangle$ is symmetric about the state with no Stark shift, $|a\rangle$. In this case the phase accumulation θ between anticrossings (for the first half cycle of the field) is given by

$$\theta=\int_{\pi/2\omega_{\mathrm{rf}}}^{3\pi/2\omega_{\mathrm{rf}}} kE_{\mathrm{rf}}\cos(\omega_{\mathrm{rf}}t)\,dt=-\frac{2kE_{\mathrm{rf}}}{\omega_{\mathrm{rf}}}. \tag{9}$$

At the second crossing we again have a Landau-Zener transition described by the evolution matrix,

$$U_{\mathrm{LZ}_2}=\begin{pmatrix} \sqrt{P} & \sqrt{1-P}e^{i\phi} \\ -\sqrt{1-P}e^{-i\phi} & \sqrt{P} \end{pmatrix}. \tag{10}$$

The outcome of this Landau-Zener transition depends on the phase θ accumulated by the two state amplitudes in between crossings, as well as the Landau-Zener phase accumulated during the transition, ϕ. For the data shown in Fig. 11(b) the phase accumulation results in constructive interference at the second crossing, and nearly all of the population is transferred to the upper state. In Fig. 11(c) we have destructive interference, which forces the population back to the initial state.

In this simple treatment the unitary transformations for the Landau-Zener transitions are written with the assumption that transitions occur only at the crossing, and the phase accumulation is written as if the states actually cross. This gives a good qualitative understanding of the data shown in Fig. 11, however, some deviations from the sharp stair steps predicted by the model can be seen. In particular, we see some oscillations where our model predicts no transitions (between crossings). These are simply off resonant transitions driven by the microwave field that are not included in this simple model.

V. THE FIELD-PHOTON CONNECTION

In the Landau-Zener model outlined above the modulation is viewed as a contribution to the static electric field that moves the system back and forth on the microwave dressed states. This is identical to the analysis used for slow modulation frequencies except that we have included the phase evolution of the states in between crossings. For slow modulations it was not necessary to include this phase since nearly all of the population was transferred between states at each avoided crossing, never leaving the system in a superposition of states with the potential for interference.

We can also apply this model in the high-frequency limit, where the rf modulation behaves more like a photon producing isolated resonances. In fact, the assumptions that were only approximately met at the end of the last section are more rigorously valid in the high-frequency regime where the avoided crossings are narrow and well separated.

By defining a single cycle propagator for our atom field system,

$$U(T,0)=U_{\theta_{23}}U_{\mathrm{LZ}_2}U_{\theta_{12}}U_{\mathrm{LZ}_1}, \tag{11}$$

and applying this propagator repeatedly,

$$\psi(t=nT)=U^n(T,0)\psi(0), \tag{12}$$

we can build up the evolution of our system one rf cycle at a time.

To find the n cycle transition probability using this single cycle propagator we follow the treatment given in Ref. [44]. We begin by multiplying out the four matrices given in Eq. (11),

$$U(T,0)=\begin{pmatrix} P+(1-P)e^{-i(\theta-2\phi)} & \sqrt{P(1-P)}(e^{-i(\theta-\phi)}-e^{-i\phi}) \\ \sqrt{P(1-P)}(e^{i\phi}-e^{i(\theta-\phi)}) & P+(1-P)e^{i(\theta-2\phi)} \end{pmatrix}. \tag{13}$$

Next, we diagonalize this matrix to find eigenvalues,

$$\lambda_{\pm}=\exp\left[\pm i[y]\arctan\left(\frac{\sqrt{1-x^2}}{x}\right)\right], \tag{14}$$

where

$$x=P+(1-P)\cos(\theta-2\phi). \tag{15}$$

In the high-frequency limit the Landau-Zener transitions are nearly diabatic so $P\approx 1$ and $\phi\approx\pi/4$. In this limit the approximations $\arctan(\gamma)\approx\gamma$ and $\sqrt{1-x^2}/x\approx\sqrt{2(1-x)}$ can be made, resulting is the simplified eigenvalues,

$$\lambda_{\pm}=\exp\left[\pm i2\sqrt{1-P}\,\cos\left(-\frac{\theta}{2}-\frac{\pi}{4}\right)\right]. \tag{16}$$

Finally, if we substitute in the expression for the Landau-Zener transition probability $P\approx 1-\pi\Omega_{\mathrm{mw}_1}^2/2k\omega_{\mathrm{rf}}E_{\mathrm{rf}}$ and the phase accumulation $\theta=-2kE_{\mathrm{rf}}/\omega_{\mathrm{rf}}$, and use the large argument form of the Bessel function, $J_0(y)=\sqrt{2/\pi y}\cos(y-\pi/4)$ we can write

$$\lambda_{\pm}=\exp\left[\pm i\pi\frac{\Omega_{\mathrm{mw}_1}}{\omega_{\mathrm{rf}}}J_0\left(\frac{kE_{\mathrm{rf}}}{\omega_{\mathrm{rf}}}\right)\right]. \tag{17}$$

Using Eq. (12) of Ref. [44] and the eigenvalues calculated above we find the time evolution of the upper state is given by

$$|b(t)|^2\propto\sin^2\left[\frac{1}{2}\Omega_{\mathrm{mw}_1}J_0\left(\frac{kE_{\mathrm{rf}}}{\omega_{\mathrm{rf}}}\right)t\right], \tag{18}$$

where we have set $t=2\pi n/\omega_{\mathrm{rf}}$. From this we can immediately see that the rf Rabi frequency for the carrier resonance considered here is identical to that given in Eq. (3),

$$\Omega_{\mathrm{rf}_0}=\Omega_{\mathrm{mw}_1}J_0\left(\frac{kE_{\mathrm{rf}}}{\omega_{\mathrm{rf}}}\right). \tag{19}$$

Note that although the derivation is not sensitive to the sign of the Rabi frequency, we have left out the absolute value signs, in part bolstered by our experimental results. The calculation of the Rabi frequency for arbitrary rf photon number q is a straightforward extension of the one presented. Although the result for the Rabi frequency is not new, as it is essentially the same result as in [32], this is the first time that it was obtained using the single cycle propagator framework.

VI. CONCLUSION

We have presented a detailed experimental study of the frequency modulated interaction with a two-level atom. By considering a broad range of frequencies of the modulation we were able to gain a basic understanding of the system in terms of some very well-known concepts such as adiabatic rapid passage, multiphoton resonances, and Landau-Zener transitions. We conclude with some comments on other systems in which there are similarities to or applications of this study.

As we stated earlier, the dressed-state anticrossing created by interaction with the microwave field is formally identical to a static field avoided crossing. In fact, such field-induced avoided crossings have been put to use in other systems. Garraway and Stenholm [45,46] have used field-induced avoided crossings to build an *interferometer within a molecule*. In this interferometer, a vibrational wave packet is split and recombined at a pair of avoided crossings to produce an interference pattern that depends on the phase accumulated between the two crossings.

Another system in which avoided crossings are familiar is the collision between a pair of atoms. By adding a field and studying radiatively assisted collisions, Renn *et al.* [42,47] have found some striking similarities to the frequency modulated interaction with a two-level atom. They use a Landau-Zener phase accumulation model to derive the cross section for the N-photon-assisted resonance.

The intuition gained from the study of simple systems and interactions like the one presented in this paper may also prove very useful in the more complicated problem of coherent control of a quantum system. The goal in coherent control is to guide the evolution of a system along a particular path to a desired final state [48–50]. Many different paradigms have been developed to perform such a task, often involving very complicated interactions. Often these *globally optimal* fields are so complicated that they would be very difficult to create experimentally. Approaching this problem from the other end by studying the frequency modulated interaction with a two-level atom is an important first step toward coherent control of more complicated systems through more complicated interactions [51,52].

ACKNOWLEDGMENTS

We thank R. R. Jones for many useful discussions. This work was supported by the U.S. Air Force Office of Scientific Research.

[1] I. I. Rabi, Phys. Rev. **51**, 652 (1937).
[2] Thomas R. Gentile, Barbara J. Hughey, Daniel Kleppner, and Theodore W. Ducas, Phys. Rev. A **40**, 5103 (1989).
[3] L. Sirko, A. Buchleitner, and H. Walther, Opt. Commun. **78**, 403 (1990).
[4] M. Gatzke, M. C. Baruch, R. B. Watkins, and T. F. Gallagher, Phys. Rev. A **48**, 4742 (1993).
[5] B. R. Mollow, Phys. Rev. **188**, 1969 (1969).
[6] F. Schuda, C. R. Stroud, Jr., and M. Hercher, J. Phys. B **7**, L198 (1974).
[7] R. E. Grove, F. Y. Wu, and S. Ezekiel, Phys. Rev. A **15**, 227 (1977).
[8] Claude Cohen-Tannoudji and Serge Reynaud, J. Phys. B **10**, 345 (1977).
[9] S. H. Autler and C. H. Townes, Phys. Rev. **100**, 703 (1955).
[10] J. L. Picqué and J. Pinard, J. Phys. B **9**, L77 (1976).
[11] C. Delsart and J-C. Keller, J. Phys. B **9**, 2769 (1976).
[12] H. R. Gray and C. R. Stroud, Jr., Opt. Commun. **25**, 359 (1978).
[13] S. Chakmakjian, K. Koch, and C. R. Stroud, Jr., J. Opt. Soc. Am. B **5**, 2015 (1988).
[14] Surya P. Tewari and M. Krishna Kumari, J. Phys. B **22**, L475 (1989).
[15] Qilin Wu, Daniel J. Gauthier, and T. W. Mossberg, Phys. Rev. A **49**, R1519 (1994).
[16] Qilin Wu, Daniel J. Gauthier, and T. W. Mossberg, Phys. Rev. A **50**, 1474 (1994).
[17] J. H. Eberly and V. D. Popov, Phys. Rev. A **37**, 2012 (1988).
[18] Surya P. Tewari and M. Krishna Kumari, Phys. Rev. A **41**, 5273 (1990).
[19] Yifu Zhu, Qilin Wu, A. Lezama, Daniel J. Gauthier, and T. W. Mossberg, Phys. Rev. A **41**, 6574 (1990).
[20] Helen Freedhoff and Zhidang Chen, Phys. Rev. A **41**, 6013 (1990).
[21] Z. Ficek and Helen Freedhoff, Phys. Rev. A **48**, 3092 (1993).
[22] M. F. Van Leeuwen, S. Papademetriou, and C. R. Stroud, Jr., Phys. Rev. A **53**, 990 (1996).
[23] S. Papademetriou, M. F. Van Leeuwen, and C. R. Stroud, Jr., Phys. Rev. A **53**, 997 (1996).
[24] S. G. Harris, M. K. Oshman, B. J. McMurty, and E. O. Amman, Appl. Phys. Lett. **7**, 185 (1965).
[25] G. C. Bjorklund, Opt. Lett. **5**, 15 (1980).
[26] Girish S. Agarwal and W. Harshawardhan, Phys. Rev. A **50**, R4465 (1994).
[27] W. Harshawardhan and Girish S. Agarwal, Phys. Rev. A **55**, 2165 (1997).
[28] Ping Koy Lam and C. M. Savage, Phys. Rev. A **50**, 3500 (1994).
[29] B. M. Garraway and N. V. Vitanov, Phys. Rev. A **55**, 4418 (1997).
[30] Maciej Janowicz, Phys. Rev. A **44**, 3144 (1991).
[31] V. N. Smelyanskiy, R. S. Conti, and G. W. Ford, Phys. Rev. A **55**, 2186 (1997).
[32] R. C. Stoneman, D. S. Thomson, and T. F. Gallagher, Phys. Rev. A **37**, 1527 (1988).
[33] E. B. Treacy, Phys. Lett. **27A**, 421 (1968).
[34] Michael M. T. Loy, Phys. Rev. Lett. **32**, 814 (1974).
[35] I. D. Abella, N. A. Kurnit, and S. R. Hartmann, Phys. Rev. **141**, 391 (1966).
[36] Y. S. Bai, A. G. Yodh, and T. W. Mossberg, Phys. Rev. A **34**, 1222 (1986).
[37] E. L. Hahn, Phys. Rev. **80**, 580 (1950).
[38] I. Solomon, Phys. Rev. Lett. **2**, 301 (1959).
[39] L. Allen and J. H. Eberly, *Optical Resonance and Two-Level Atoms* (Dover Publications, New York, 1987).
[40] E. E. Nikitin and S. Ya. Umanskii, *Theory of Slow Atomic Collisions* (Springer-Verlag, Berlin, 1984).
[41] M. Gatzke, R. B. Watkins, and T. F. Gallagher, Phys. Rev. A **51**, 4835 (1995).
[42] M. J. Renn, D. S. Thomson, and T. F. Gallagher, Phys. Rev. A **49**, 409 (1994).
[43] Jan R. Rubbmark, Michael M. Kash, Michael G. Littman, and Daniel Kleppner, Phys. Rev. A **23**, 3107 (1981).
[44] W. M. Griffith, Michael W. Noel, and T. F. Gallagher, Phys. Rev. A **57**, 3698 (1998).
[45] B. M. Garraway and S. Stenholm, Opt. Commun. **83**, 349 (1991).
[46] B. M. Garraway and S. Stenholm, Phys. Rev. A **46**, 1413 (1992).
[47] M. J. Renn and T. F. Gallagher, Phys. Rev. Lett. **67**, 2287 (1991).
[48] Paul Brumer and Moshe Shapiro, Acc. Chem. Res. **22**, 407 (1989).
[49] W. S. Warren, H. Rabitz, and M. Dahleh, Science **259**, 1581 (1993).
[50] D. Neuhauser and H. Rabitz, Acc. Chem. Res. **26**, 496 (1993).
[51] J. S. Melinger, Suketu R. Gandhi, A. Hariharan, J. X. Tull, and W. S. Warren, Phys. Rev. Lett. **68**, 2000 (1992).
[52] N. V. Vitanov and P. L. Knight, Opt. Commun. **121**, 31 (1995).